

Accelerating cryoprotectant delivery using vacuum infiltration

Ryan J. Forcier^a, Robert T. Heussner^a, Lauren Newsom^b, Morgan B. Giers^a,
Wa'el Al Rawashdeh^c, Kimberly A. Buchanan^c, Erik J. Woods^c, Brian H. Johnstone^c,
Adam Z. Higgins^{a,*}

^a School of Chemical, Biological and Environmental Engineering, Oregon State University, Corvallis, OR, USA

^b Department of Clinical Sciences, Carlson College of Veterinary Medicine, Oregon State University, Corvallis, OR, USA

^c Ossium Health, Inc., Indianapolis, IN, USA

ARTICLE INFO

Keywords:

Vertebral body
Tissue
Organ
Mass transfer
Cryoprotectant
Vacuum

ABSTRACT

The ability to cryopreserve bone marrow within the vertebral body (VB) would offer significant clinical and research benefits. However, cryopreservation of large structures, such as VBs, is challenging due to mass transport limitations that prevent the effective delivery of cryoprotectants into the tissue. To overcome this challenge, we examined the potential of vacuum infiltration, along with carbonation, to increase the penetration of cryoprotectants. In particular, we hypothesized that initial exposure to high-pressure carbon dioxide gas would introduce bubbles into the tissue and that subsequent vacuum cycling would cause expansion and contraction of the bubbles, thus enhancing the transport of cryoprotectant into the tissue. Experiments were carried out using colored dye and agarose gel as a model revealing that carbonation and vacuum cycling result in a 14% increase in dye penetration compared to the atmospheric controls. Experiments were also carried out by exposing VBs isolated from human vertebrae to 40% (v/v) DMSO solution. CT imaging showed the presence of gas bubbles within the tissue pores for carbonated VBs as well as control VBs. Vacuum cycling reduced the bubble volume by more than 50%, most likely resulting in replacement of this volume with DMSO solution. However, we were unable to detect a statistically significant increase in DMSO concentration within the VBs using CT imaging. This research suggests that there may be a modest benefit to carbonation and vacuum cycling for introduction of cryoprotectants into larger structures, like VBs.

1. Introduction

Cryopreservation of biological specimens has meaningful implications in many fields. For example, cryopreservation in reproductive medicine has enabled the storage of gametes and embryos, improving assisted reproduction [1,34,36,47]. Cryopreservation has also been applied to more complex specimens, facilitating storage prior to allotransplantation of articular cartilage in humans, whole ovaries in rats, and kidneys in rabbits [13,17,43]. While there are examples of successful cryopreservation of tissues and organs, most are found in small animal models and it remains one of the major challenges in cryobiology to routinely cryopreserve complex tissues and organs successfully [18, 32].

Many of the examples of successful tissue and organ cryopreservation employ vitrification methods. Vitrification involves solidification of the sample without the formation of ice crystals. This is achieved using

fast cooling rates and high cryoprotectant (CPA) concentrations to promote formation of a glassy phase. Several issues exist with vitrification methods. The high CPA concentrations needed are usually toxic and often need to be introduced gradually in a stepped manner [16,28, 45]. Additionally, the significant volume of tissues and organs represents a major issue for heat transport. Using fast cooling rates applied to the boundaries of a specimen will lead to large thermal gradients and non-uniform cooling rates within the specimen. It is also possible for thermal stress to cause damage, such as fractures [22].

The classical method of cryopreservation, slow cooling, involves some degree of crystallization. Ice crystals first nucleate in the extracellular medium when the temperature drops, which increases the solute concentration and creates an osmotic driving force for water to leave the cell, increasing the intracellular concentration as well. If sufficient intracellular water is removed during slow cooling, then the sample can be transferred to cryogenic temperatures without formation of

* Corresponding author.

E-mail address: adam.higgins@oregonstate.edu (A.Z. Higgins).

<https://doi.org/10.1016/j.cryobiol.2023.104558>

Received 9 March 2023; Received in revised form 22 June 2023; Accepted 11 July 2023

Available online 13 July 2023

0011-2240/© 2023 The Authors. Published by Elsevier Inc. This is an open access article under the CC BY license (<http://creativecommons.org/licenses/by/4.0/>).

intracellular ice. CPAs are typically added to help suppress intracellular ice formation and reduce solution effects damage from the freeze-concentrated extracellular solution.

One problem common to both slow cooling and vitrification approaches is mass transport limitations. Both strategies rely on CPAs to be effective, but it is a challenge to introduce CPAs into large 3D volumes in an appropriate timeframe. In some cases, it is possible to improve mass transport by perfusing CPA throughout a specimens vasculature [13,17]; however, perfusion is not feasible for all tissues and organs. This is particularly true for cartilaginous tissues such as articular cartilage, meniscus, and the intervertebral disc.

Another example of such a tissue is the vertebral body (VB). The VB is the thick cylindrical segment of bone forming the anterior portion of the vertebrae. It consists of cancellous bone tissue filled with bone marrow and encompassed by a thin layer of cortical bone. Vertebral bone marrow contains large quantities of hematopoietic stem and progenitor cells (HSPCs) and mesenchymal stem cells (MSCs) [23,25,26]. With more than 10,000 deceased organ donors in the US annually [12], the banking of cryopreserved VBs could meet much of the demand for HSPCs and MSCs in clinical settings such as tolerance induction following organ transplantation [48], or HSPC transplantation [9]. Cryopreservation of deceased donor vertebral bone marrow *in situ* would allow for banking of HSPCs and MSCs without grinding and isolating the functional fraction of bone marrow before an immunocompatible match is found. By waiting to isolate cells until a compatible recipient is determined, the banking process becomes less time intensive and more cost effective. One significant challenge that needs to be overcome for cryopreservation of VBs is the loading of CPA. It is impractical to deliver CPA by perfusion through the vasculature. Each VB would need to be cannulated and perfused individually, which would be excessively labor intensive and costly. Moreover, standard diffusion protocols would take several hours to reach any meaningful concentration in the center. Novel methods of CPA loading are needed for the optimal cryopreservation of larger structures, like VBs.

Towards that end, this study examines vacuum infiltration as an approach to increase CPA penetration into 3D structures. This work is motivated by numerous studies in food sciences and agriculture which have shown that vacuum infiltration can successfully aid penetration of small molecules for storage [11,33], and vitamin enrichment [14], of fruits and vegetables. Vacuum infiltration has also been explored for seafood freshness [41], and meat marination [19], with varying levels of success. In cryobiology, there are a small number of studies suggesting that vacuum treatment may be beneficial. Cryopreservation of grape buds was reported to be improved following a single vacuum treatment which led to increased CPA concentration compared to passive atmospheric controls [35]. Soejima et al. [39] used vacuum infiltration for CPA loading in cryopreservation of a rat hindlimb model, resulting in slight improvement in preservation when vacuum was applied based on qualitative assessment of histology images. Toyama-Mori et al. [42] recently reported faster penetration of cryoprotectant into ovarian tissue when a vacuum was applied, resulting in improved results after cryopreservation.

From previous investigations in food sciences, it has been shown that vacuum infiltration impacts the loading of solutions through a “hydrodynamic mechanism” based on the porous structure of many foods [20, 21,30,31,38,41]. When vacuum is applied, gas expands in internal pores forcing fluid out of the sample. When atmospheric pressure is restored, the gas contracts, which pulls external solution into the specimen. Since gases play an important role in this phenomenon, increasing the amount of gas present, either dissolved or aggregated as bubbles, should have a positive impact on the efficacy of vacuum infiltration. One possible approach to increase the amount of internal gas is to expose the sample to a high pressure of a relatively soluble gas, such as carbon dioxide. Carbon dioxide is routinely used in carbonated beverages, and it has even been used to introduce bubbles into whole fruits, but, to our knowledge, carbonation has not previously been examined as a

preliminary step prior to vacuum infiltration.

In this study, we examine the hypothesis that vacuum infiltration, in combination with carbonation, improves CPA loading. To test this hypothesis, experiments were performed using human VBs, as well as agarose gel, which was used as a model tissue. To monitor the distribution of DMSO within VBs both spatially and temporally we turned to computed tomography (CT), an imaging method that has been used before to measure DMSO concentration in soft tissues [2,7]. CT imaging was also used to quantify bubbles within the VBs. Our results shed light on the effects of vacuum and carbonation on CPA penetration into tissues, which has important implications for cryopreservation of VBs and other large tissues and organs.

2. Methods and Materials

2.1. Vacuum cycling apparatus

The general setup for applying a vacuum to the samples consisted of a vacuum pump, pressure gauge, desiccator chamber, and a valve to control pressure (Fig. 1a). The vacuum apparatus setup differed slightly for different experiments.

For experiments with agarose (see Section 2.2), an E2M1.5 rotary vacuum pump (Edwards, West Sussex, UK) was connected to a bleed valve (LV10K, Edwards, West Sussex, UK), and pressure gauge (APG100-XLC, Edwards, West Sussex, UK), through an aluminum cross piece. The desiccator was connected via ¼” I.D. plastic tubing. Vacuum cycling was controlled manually. Fig. 1b depicts a representative plot of the pressure cycling for a 6-cycle vacuum treatment. The bleed valve was set so that an absolute pressure of 23 mmHg was achieved under vacuum. This pressure was selected as it is slightly higher than the vapor pressure of water at room temperature (approximately 18 mmHg), meaning that 23 mmHg is the strongest vacuum that can be pulled without boiling the solution. The accuracy of the pressure gauge was validated by closing the bleed valve and confirming that the gauge read 18 mmHg when the water started to boil.

For experiments with VBs (see section 2.3), a less powerful vacuum pump was used to apply gentler vacuum pressures. The vacuum pump (Cell culture aspiration station 2515, Welch, Prospect, IL) contains an integrated valve to control pressure and integrated pressure gauge which was used to measure the vacuum achieved. For VB dye uptake experiments, an absolute pressure of 300 mm Hg was used, and vacuum cycling was controlled manually. For CT imaging, it was necessary to automate vacuum cycling. A solenoid valve (PV16EKA, Edwards, West Sussex, UK) was connected to a data acquisition (DAQ) device (NI USB-6210, National Instruments, Austin, TX) allowing for the automation of the open/close signal using MATLAB (R2020b, MathWorks, Natick, MA). The connections between components were similar to those described in Fig 2.1a with the solenoid valve connected to the aluminum cross piece instead of the bleed valve. For these CT experiments, an absolute pressure of 260 mm Hg was used.

2.2. Agarose experiments

To examine the effects of carbonation and vacuum cycling, experiments were performed to assess the uptake of a colored dye into agarose gel cylinders. Agarose gel was chosen for its replicability and frequent use as a model of soft tissue [40]. The agarose cylinders ($n = 91$) were divided into seven groups, 13 cylinders each, and subjected to the treatments described below.

Baseline control. Cylinders were not exposed to dye solution and acted as a zero baseline for absorbance measurements.

Fully equilibrated control. Cylinders were placed in dye solution for 24 h, representing the maximum amount of dye that could be loaded into an agarose cylinder.

Non-carbonated atmospheric. Cylinders were placed in dye solution for 30 min under atmospheric pressure. This group measured the impact

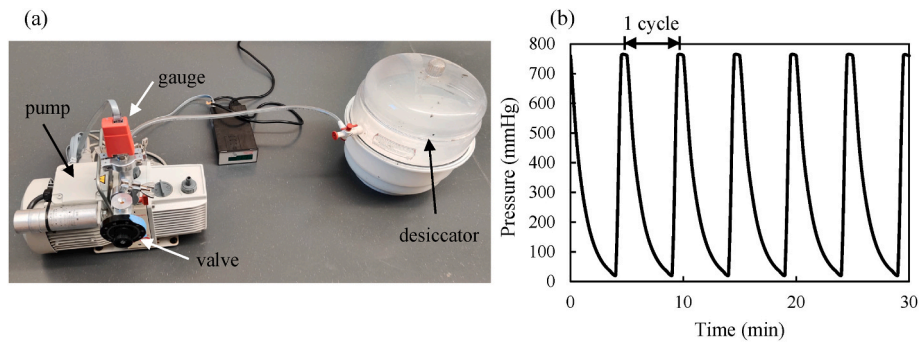


Fig. 1. (a) Image of the vacuum apparatus used in agarose experiments. A vacuum pump creates a vacuum within the desiccator and the bleed valve is used to control the level of vacuum which is measured by the pressure gauge. (b) Representative pressure versus time for a 6-cycle vacuum treatment.

of diffusion alone on dye loading.

Carbonated atmospheric. Cylinders were carbonated and then placed in dye solution for 30 min under atmospheric pressure. This group examined the effects of carbonation on dye loading.

Non-carbonated vacuum cycling. Cylinders were placed in dye solution and subjected to 30 min of vacuum cycling (six cycles consisting of 4 min under vacuum and 1 min without vacuum). This group assessed the effects of vacuum cycling on dye loading.

Carbonated vacuum cycling. Cylinders were carbonated and then placed in dye solution and subjected to vacuum cycling for 30 min (six cycles consisting of 4 min under vacuum and 1 min without vacuum). This group examined the combined effects of carbonation and vacuum cycling on dye loading.

Carbonated constant vacuum. Cylinders were carbonated and then placed in dye solution and subjected to a constant vacuum for 29 min followed by 1 min without vacuum. This group was used to investigate the impact of the number of cycles between atmospheric and vacuum pressures.

2.2.1. Agarose preparation

The agarose gel was prepared using high gelling temperature agarose powder (Bethesda Research Laboratories, Gaithersburg, MD) in 3.7 g/L sodium bicarbonate buffer (EMD Millipore, Burlington, MA). Agarose was slowly combined with the buffer while stirring to achieve a final concentration of 2% w/v. The solution was heated, with continuous stirring, on a hot plate at 120 °C until the solution turned entirely transparent. The solution was then poured into a circular polypropylene container to a layer thickness of 2 cm. The container was left at room temperature and allowed to cool until the agarose gel had completely solidified at which point it was stored at 4 °C. Agarose cylinders were made using a cork borer giving a cylinder diameter of 1 cm.

2.2.2. Dye solution

In order to quantify the penetration of solute into agarose gel, a blue dye solution was used. Dye solution was prepared using a pH 7.3 phosphate buffer made from 1.15 g/L $\text{Na}_2\text{HPO}_4 \cdot 7\text{H}_2\text{O}$ (Macron Fine Chemicals, Radnor, PA) and 0.2 g/L KH_2PO_4 (Mallinckrodt Chemicals, Phillipsburg, PA). Blue food dye, containing FD&C Blue #1, was added to the phosphate buffer resulting in a stock solution with absorbance of 2.1 at 630 nm using a cuvette with a 1 cm path length. This stock solution concentration was chosen as it resulted in absorbance values on the lower half of the linear range when diluted during the experimental procedure.

2.2.3. Carbonation of agarose cylinders

To carbonate the agarose, cylinders were placed into 500 mL Nalgene™ high-density polyethylene (HDPE) bottles along with approximately 5 g dry ice for 12 h. This amount of dry ice is expected to provide a CO_2 partial pressure of approximately 5.5 atm within the container. Lids were sealed using silicone vacuum grease and screwed on tightly.

Damp paper towels were also placed in the bottles between the dry ice and agarose cylinders to prevent direct contact which could freeze the cylinders. Cylinders used in non-carbonated groups were also placed in bottles with a damp paper towel, without dry ice, for 12 h at room temperature.

2.2.4. Quantifying dye uptake

Agarose cylinders were placed in 50 mL of dye solution and subjected to the appropriate treatment. Immediately following completion of the treatment, cylinders were briefly blotted dry to remove excess liquid. Twelve cylinders were placed individually in 5 mL deionized (DI) water for 24 h to allow for equilibration between the DI water and the dye that had penetrated the cylinder. The remaining one cylinder was sacrificed for a cross-sectional slice from the middle for imaging. After 24 h, the absorbance of the equilibrated solution was measured using a spectrophotometer (Nicolet Evolution 100, Thermo Electron, Waltham, MA) at a wavelength of 630 nm [15]. Absorbance was normalized to the fully equilibrated control to represent how much dye had penetrated into the agarose cylinder compared to a fully loaded sample.

2.3. VB experiments

Experiments were performed with human VBs to assess the effects of carbonation and vacuum cycling on solute penetration. To qualitatively examine solute penetration, VBs were placed in dye solution and the distribution of dye within the VB was visualized by cutting the VB in half and taking an image. For more quantitative analysis of solute penetration, CT was used to acquire images of VBs in DMSO solution.

2.3.1. VB acquisition

VB specimens were acquired following previously developed clinical recovery methods [46]. Vertebral sections were acquired from deceased donors who had consented to be organ and tissue donors by a licensed Organ Procurement Organization using an IRB approval protocol. Vertebral sections were then shipped to Ossium Health where all specimen processing occurred. Specimen processing involved soft tissue debridement, removal of the pedicles from the vertebral body, and separation from the intervertebral discs leaving clean, separated VBs. Processed VBs were wrapped in lap sponges soaked in saline and placed in double-sealed bags to ensure moisture retention and stored at 4 °C for up to 24 h before shipping.

2.3.2. VB dye experiments

VBs were subjected to either atmospheric conditions or vacuum cycling with or without carbonation. VBs used in atmospheric treatments were taken from one donor while VBs used in the vacuum treatments came from a second donor. Individual VBs were placed in plastic beakers on their edge, posterior side up, along with approximately 100 mL of 0.5% crystal violet dye solution (MilliporeSigma, Burlington, MA) so that each VB was fully submerged. VBs in dye solution were then

subjected to the treatments described below.

Non-carbonated atmospheric. VBs were placed in dye solution and remained under atmospheric conditions for 30 min, 3 h, or 72 h. This provides a baseline for the impact of diffusion under atmospheric conditions on dye infiltration.

Non-carbonated vacuum cycling. VBs were placed in dye solution and subjected to five cycles consisting of 2 min under vacuum and 2 min without vacuum. This examines how vacuum cycling impacts dye infiltration.

Carbonated vacuum cycling. VBs were carbonated and then placed in dye solution and subjected to five cycles consisting of 2 min under vacuum and 2 min without vacuum. This examines the combined effects of carbonation and vacuum cycling on dye infiltration.

VBs in the carbonated vacuum cycling group were carbonated by placing the VBs in plastic beakers on the bottom of a 16-quart hard-sided cooler followed by adding approximately 2 kg of dry ice around the beakers. The cooler was then wrapped with plastic wrap to reduce gas leakage. After 1 h, the VBs were removed from the cooler, placed in dye solution, and subjected to vacuum cycling as described above.

Following completion of the treatment, VBs were removed from the dye solution and blotted dry to remove excess solution. VBs were then cut in half along the sagittal plane and the interior surface was imaged to observe dye penetration through the cross-section.

2.3.3. Experimental design for CT imaging

CT imaging was used to measure gas bubble volume within the VBs before and after carbonation, and to measure the DMSO concentration in the VBs after exposure to 40% (v/v) DMSO under various conditions. Wrapped specimens were shipped from Ossium Health to Oregon State University overnight on ice for CT imaging. In total, two donors (Donor 1 and Donor 2) contributed 8 VBs each for a total of 16 VBs. Upon receipt, VBs remained wrapped in lap sponges soaked in saline, sealed in bags to ensure moisture retention, and stored at 4 °C overnight. The following morning, VBs were removed from packaging and VB mass was measured. The VBs were then assigned to treatment conditions using their mass to randomize their assignment. The lightest VB from each donor was designated as VB 1 while the heaviest was VB 8. VBs 1–4 and 5–8 from each donor were then randomly assigned to one of four treatment groups:

Non-carbonated atmospheric. VBs were exposed to DMSO under atmospheric conditions. This provides a baseline for the impact of diffusion under atmospheric conditions on DMSO infiltration.

Carbonated atmospheric. VBs were carbonated and then exposed to DMSO under atmospheric conditions. This examines the effects of carbonation on DMSO infiltration under atmospheric conditions.

Non-carbonated vacuum cycling. VBs were exposed to DMSO and subjected to three cycles consisting of 8 min under vacuum and 2 min without vacuum. This examines how vacuum cycling impacts DMSO infiltration.

Carbonated vacuum cycling. VBs were carbonated and then exposed to DMSO and subjected to three cycles consisting of 8 min under vacuum and 2 min without vacuum. This examines the combined effects of carbonation and vacuum cycling on DMSO infiltration.

2.3.4. CT imaging

CT images were acquired using a 64-slice helical scanner (Toshiba Aquilion, Toshiba America Medical Systems, Tustin, CA) with the following parameters: 120 kVp, 250 mA, and pitch of 0.6. Images were reconstructed into 0.5 mm slices, with pixel dimensions of $0.47 \times 0.47 \text{ mm}^2$, in a high frequency algorithm and were viewed in a bone window.

For all CT scans, VBs were placed in polypropylene beakers on the CT bed. A total of 10 scans were taken of each VB. An initial scan was taken after receiving VBs at Oregon State University prior to any treatment. This initial CT scan was used to calculate VB volume as well as act as a baseline for gas bubble volume. The following day, either after carbonation or storage, an additional scan was taken. Then VBs were

immersed in DMSO solution, and scans were taken at 5 min intervals for 30 min. VBs in vacuum treatment groups were in the desiccator chamber on the CT bed, while the atmospheric VBs were placed on the CT bed next to the desiccator. Following the 30-min scan, all VBs were stored in the DMSO solution at 4 °C and were scanned at 1-week and 4-week follow-ups. At 4 weeks, it was assumed that the pore space within the VBs had completely equilibrated with the 40% DMSO solution. This is a reasonable assumption, as diffusion calculations suggest nearly complete equilibration within two weeks.

PBS and 40% DMSO solutions were included in the scans to provide a consistent image control between scans. As shown in the Appendix (Fig. A3), when multiple scans were taken on the same day, the PBS and DMSO solution controls yielded consistent results. There was slight variability between scans taken on different days, but the differences are expected to have a negligible effect on the results.

The 40% DMSO solution was made using DMSO (VWR Chemicals BDH, Radnor, PA) in phosphate-buffered saline (PBS) at physiological osmolarity. The PBS was made using: 8 g/L NaCl (VWR Chemicals BDH, Radnor, PA), 1.15 g/L $\text{Na}_2\text{HPO}_4 \cdot 7\text{H}_2\text{O}$ (Macron Fine Chemicals, Radnor, PA), 0.2 g/L KH_2PO_4 (Mallinckrodt Chemicals, Phillipsburg, PA), and 0.2 g/L KCl (EMD Millipore, Burlington, MA). The solution was pH-adjusted to 7.3 ± 0.1 .

VBs in the carbonated treatment groups were carbonated for 12 h by placing approximately 1 kg dry ice in the bottom of a 16-quart hard-sided cooler followed by a layer of room temperature gel packs with the VBs in plastic beakers resting on top of the gel packs. The gel packs served as a physical and thermal buffer to avoid freezing the VBs. The cooler was then wrapped with plastic wrap to reduce gas leakage. The non-carbonated VBs were wrapped in lap sponges soaked with saline and stored at 4 °C.

To confirm a linear trend between X-ray attenuation and DMSO concentration, a standard curve was created using DMSO solutions with concentrations ranging from 0% to 60% (v/v). To make the measurements, 1 mL of each solution was placed in a well of a 24-well plate, in triplicate, and imaged in CT. To make the standard curve, the average grayscale value of the solution volume in each well was obtained from the CT images. The X-ray attenuation proved to be proportional to the DMSO concentration (Fig. A1), as has been published previously [6,7]. We also confirmed that the DMSO concentration within VBs could be estimated from the X-ray attenuation by equilibrating VBs in a range of DMSO concentrations for four weeks (Fig. A2). The DMSO concentration within the VBs was estimated using equation (A1), which accounts for tissue porosity. The resulting estimates matched the external DMSO concentration in the solution around the VBs, as expected.

2.4. Image processing

The CT scans (Fig. 2a) in their original Digital Imaging and Communications in Medicine (DICOM) format were imported into Mimics software (version 23.0, Materialise, Leuven, Belgium). Segmentation of individual VBs was performed by thresholding at an intensity associated with bone (226–3071 Hounsfield units) and then isolating each VB as a separate 3D object. Holes and protuberances in the masks for each object were removed by morphologically closing, then opening the image slice by two pixels in 26-connectivity, followed by cleaning remaining mask defects. From the VB segments, 3D objects were created (Fig. 2b), and a 3D smoothing operation was applied (smoothing factor of 0.6 and iteration count of 4) to the object surface. Final 2D VB masks were made from the smoothed 3D objects which closely followed the borders of the VBs.

The VB masks were imported into ImageJ (version 1.53c, <https://imagej.nih.gov/ij/>) and multiplied by the original 16-bit grayscale CT images (Fig. 2c). Masked CTs were converted to 8-bit images and thresholded at an intensity of 50 to capture air bubbles (Fig. 2d). Bubble masks were used to calculate bubble volume by multiplying the number of pixels by the voxel size. CT scans were used to estimate DMSO

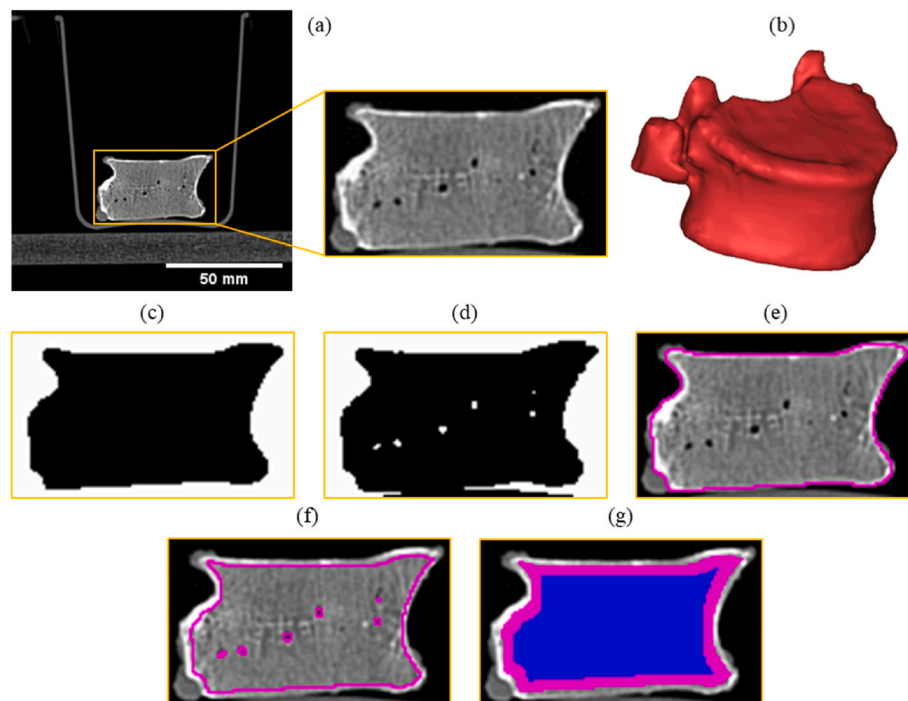


Fig. 2. (a) CT scan slice with close-up of the VB of interest, (b) smoothed 3D object, (c) binary VB mask, (d) binary gas bubble mask, (e) ROI (purple outline) of the whole VB, (f) ROI of the combined VB and gas bubble masks, (g) inner (blue) and outer (purple) regions of the VB. (For interpretation of the references to color in this figure legend, the reader is referred to the Web version of this article.)

concentration as follows. For each VB, the VB mask was used to measure the area of each slice (Fig. 2e), which was multiplied by slice thickness and summed to give the volume of the whole VB. VB masks were then eroded twice in order to exclude the majority of cortical bone around the edges of the VB and the volume was measured again. Cortical bone was excluded due to its low porosity and high attenuation which would make changes in intensity due to DMSO undetectable. The VB masks and gas bubble masks were combined using a Boolean AND operation resulting in an ROI encompassing the VB without air pockets (Fig. 2f). Using this combined ROI, the area and mean pixel intensity for each slice was measured and the volume of the eroded VB excluding gas bubbles was determined. A single volume-averaged intensity was determined for each VB according to the following equation:

$$\bar{I} = \frac{\sum_{i=1}^n (I_i A_i)}{\sum_{i=1}^n A_i} \quad (1)$$

where \bar{I} is the average VB intensity, I_i is the mean pixel intensity within the ROI for each slice and A_i is the area of each slice. To see if there were differences in DMSO concentration between the inner and outer portions of the VB, the VB masks were split into an inner and outer region and the intensities of these regions were measured at 0- and 30-min time points (Fig. 2g). The inner region was created by eroding the VB mask using a disk structure element with a radius of 3 pixels.

The DMSO concentration was estimated for each VB using the assumption that at 4 weeks, the exchangeable volume in the pore space had equilibrated with the external 40% DMSO solution. Therefore, we assumed that the change in intensity between the 0-min and 4-week time point was a result of the 40% DMSO solution, allowing calculation of the DMSO concentration in the VB at any time point t :

$$\text{DMSO Concentration} = 40\% * (\bar{I}_t - \bar{I}_0) / (\bar{I}_{4\text{-week}} - \bar{I}_0) \quad (2)$$

where \bar{I}_t is the volume averaged intensity at a given time, \bar{I}_0 is the initial intensity at the 0-min time point, and $\bar{I}_{4\text{-week}}$ is the intensity at 4 weeks.

2.5. Statistical analysis

Statgraphics software (Statgraphics Technologies, Inc., The Plains, VA) was used to perform all statistical analysis. One-way ANOVA was used in the comparisons of dye absorbance in agarose experiments, VB mass and volume between donors, as well as gas bubble volumes, and DMSO concentrations after 30 min in VB experiments. Two-way ANOVA was used to compare DMSO concentrations between the inner and outer VB regions. Fischer's least significant difference (LSD) test was used post hoc for all pairwise comparisons. A paired t -test was used to compare air bubble volume before and after 12-h treatment using either carbon dioxide gas or air at atmospheric conditions. Linear regression analysis was used to determine if DMSO concentration increased across time points over 30 min. Values of $p < 0.05$ were considered statistically significant. Values are reported as mean \pm standard error of the mean (SEM).

3. Results

3.1. Effects of carbonation and vacuum cycling on dye penetration into agarose gel cylinders

To quantify the factors affecting solute penetration, experiments were performed using agarose gel as a model tissue. Of particular interest were the role that carbonation and vacuum cycling played on solute infiltration compared to atmospheric conditions. Solute infiltration was quantified by placing agarose samples in a solution of blue dye, then transferring the samples to water and measuring the release of dye into the water by spectrophotometry.

The absorbance values for each treatment were normalized to the positive control group that had been equilibrated in the dye solution for 24 h, resulting in the normalized absorbance values shown in Fig. 3. While there were statistically significant differences between treatments ($p = 0.0001$), the effects were modest. All treatment groups yielded a similar extent of dye uptake ranging from 33% to 38% of the fully equilibrated control. On its own, carbonation did not result in a

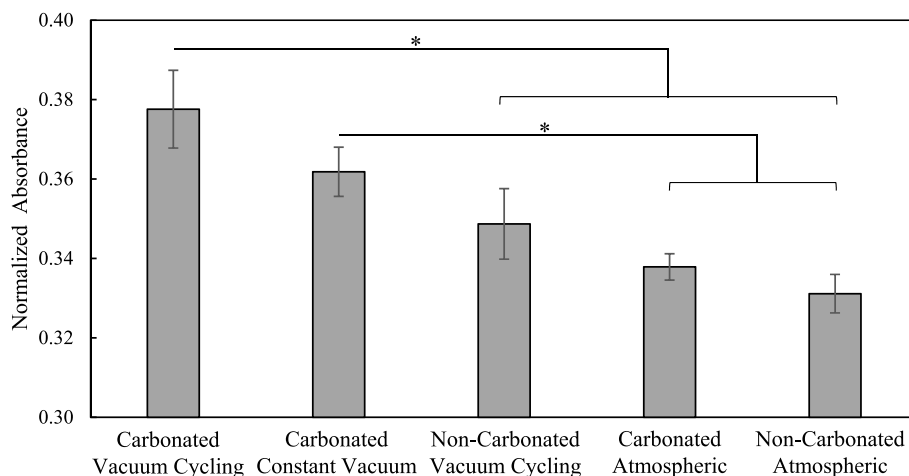


Fig. 3. Infiltration of dye into agarose cylinders after 30 min. Agarose cylinders were subjected to the following conditions during the 30 min dye uptake period: atmospheric pressure with and without prior carbonation, cycling between vacuum and atmospheric pressure six times with and without carbonation, and exposure to constant vacuum with prior carbonation. * indicates statistically significant difference ($p < 0.05$).

significant increase in dye uptake, evidenced by the similar absorbance of the atmospheric groups with and without carbonation. Additionally, vacuum cycling on its own did not lead to a significant increase in dye uptake. However, the combination of carbonation and vacuum cycling did lead to a statistically significant increase in dye uptake for both the 6-cycle and 1-cycle vacuum treatments compared to atmospheric controls. The largest increase in dye uptake was seen between the carbonated, 6-cycle vacuum treatment and non-carbonated atmospheric control with an improvement of 14%. Further, carbonation followed by six cycles of vacuum resulted in a statistically significantly increase in dye uptake over the same vacuum treatment without carbonation.

While the absorbance values show improved dye infiltration following carbonation and vacuum cycling, inspection of the cross-sectional slice images revealed no obvious qualitative differences

between the different treatment groups. The top panels of Fig. 4 show the baseline (dye-free) control as a transparent circle and the fully equilibrated control as a circle with uniform blue color. The remaining treatment groups show incomplete penetration of the dye, with a faint gradient in the radial direction and no obvious differences between atmospheric and vacuum-cycled groups (Fig. 4c and d).

3.2. Effects of carbonation and vacuum cycling on dye penetration into VBs

The goal of this study was to examine the impact of carbonation followed by application of vacuum on CPA loading in VBs. To test this, initial experiments were performed by placing VBs in a solution containing crystal violet dye, followed by transection of the VBs to assess

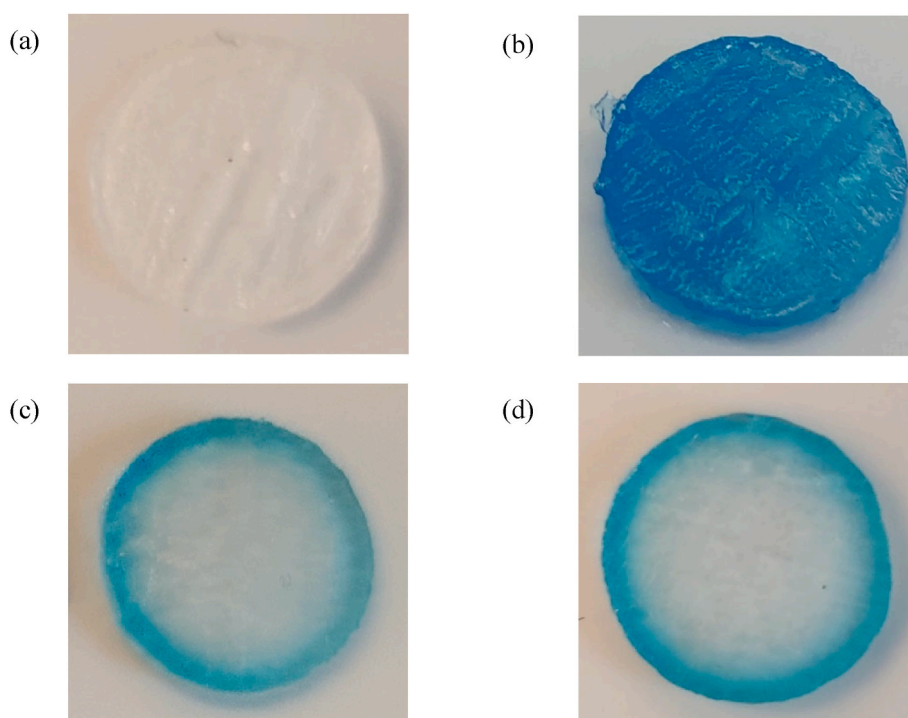


Fig. 4. Representative photos from the middle of the agarose cylinders for the (a) dye-free control, (b) fully equilibrated control, (c) non-carbonated, atmospheric treatment, and (d) carbonated, vacuum cycling treatment.

dye penetration. The top panels of Fig. 5 show the diffusion of crystal violet dye into whole VBs under atmospheric conditions. In both the 30-min and 3-h VBs, there is a cavity in the side of the VBs that allowed for some dye to penetrate, though it is localized to the area immediately near the cavity. There was no noticeable penetration of dye into the interior regions of the VB after 72 h. The bottom panels of Fig. 5 show the infiltration of dye after vacuum cycling by itself or combined with carbonation. In marked contrast to the atmospheric controls, the presence of dye pockets in the inner regions of the VB suggest that vacuum cycling does have an impact on the penetration of solutes into the VBs. The extent of dye penetration was similar for VBs subjected to vacuum cycling with and without carbonation. Overall, these qualitative results support the idea that vacuum infiltration can be used to increase solute penetration into VBs.

3.3. Effects of carbonation and vacuum cycling on DMSO infiltration into VBs

The dye uptake experiments for VBs and agarose discs suggest a possible benefit of carbonation and vacuum cycling for CPA loading in 3D structures. To investigate this, we used CT imaging to examine the effects of carbonation and vacuum cycling on DMSO penetration into VBs. CT imaging was also used to measure gas bubble volumes within VBs.

The characteristics of the VBs used in CT imaging are summarized in Table 1. VB volume was estimated from initial CT scans prior to any treatment. VBs from donor 2 were smaller as evidenced by smaller mass ($p = 0.0001$) and volume ($p = 0.0003$). However, the density (VB mass/VB volume) for both donors was similar ($p = 0.76$).

To test whether carbonation increased the volume of gas bubbles within the VB, the volume of bubbles was measured before and after carbonation. As shown in Fig. 6a, the gas bubble volume increased by nearly a factor of four after carbonation. As a control, Fig. 6a also shows the gas bubble volume in VBs that were maintained under atmospheric conditions for the same amount of time as the carbonation treatment. In

Table 1

Mean (\pm SEM) values for mass, volume, and density of VBs by donor ($n = 8$).

Donor	Mass (g)	Volume (cm^3)	Density (g/cm^3)
1	33.3 (± 1.6) ^a	23.8 (± 1.5) ^a	1.41 (± 0.03) ^a
2	19.3 (± 2.0) ^b	13.6 (± 1.5) ^b	1.42 (± 0.02) ^a

^{a,b} Means differ significantly between donors if they do not share a common superscript letter.

this case, the gas bubble volume went down ($p = 0.03$), potentially as a result of the gas in the bubbles dissolving into the fluid within the VBs. This shows that the increase in gas volume after carbonation can be attributed to the carbonation process, and not simply to natural changes in bubble volume occurring over time.

To examine the impact of vacuum on the gas bubbles within the VBs, the volume of gas bubbles was measured before and after 30 min of vacuum treatment. As shown in Fig. 6b, the bubble volume significantly decreased after vacuum treatment. This was true for both vacuum treated groups (with and without carbonation). In contrast, the atmospheric control showed no appreciable change in bubble volume after 30 min, and the carbonated atmospheric treatment actually exhibited a slight increase in bubble volume, likely a result of dissolved carbon dioxide coming out of solution over the 30 min to form additional gas bubbles. Taken together, these results demonstrate that vacuum treatment decreases bubble volume, suggesting that application of vacuum causes gas bubbles to expand and flow out of the VB.

To investigate the time course of bubble volume change during vacuum cycling, the bubble volumes were measured at 0, 5, 10, 15, 20, and 30 min. Fig. 6c shows the gas volumes over the 30 min, normalized to the 0-min time point. The gas volume remains unchanged in the non-carbonated atmospheric group demonstrating that gas volume is relatively stable over short time periods. The carbonated atmospheric treatment shows a consistent trend of increasing bubble volume over the 30 min consistent with carbon dioxide continually coming out of solution to contribute to bubble volume. Interestingly, both vacuum-treated

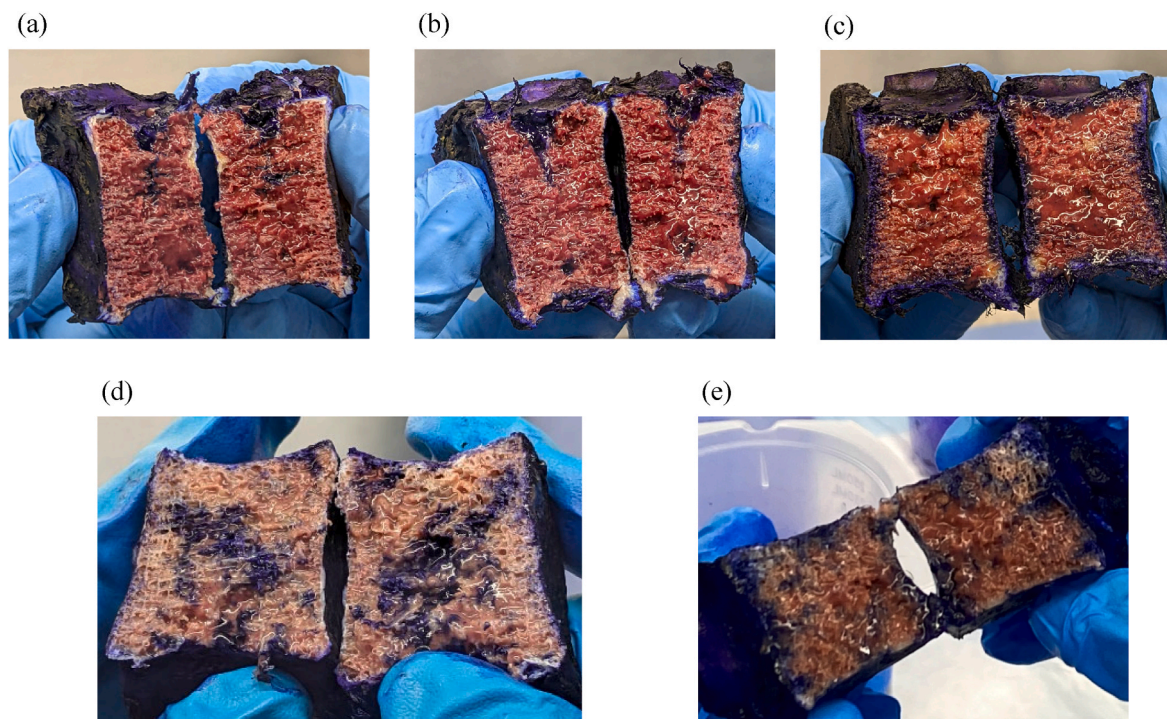


Fig. 5. Representative images of VBs cut in half after being removed from crystal violet dye following (a) a 30-min soak under atmospheric conditions ($n = 3$), (b) a 3-h soak under atmospheric conditions ($n = 3$), (c) a 72-h soak under atmospheric conditions ($n = 3$), (d) five cycles of vacuum ($n = 1$), and (e) carbonation and five cycles of vacuum ($n = 1$). (For interpretation of the references to color in this figure legend, the reader is referred to the Web version of this article.)

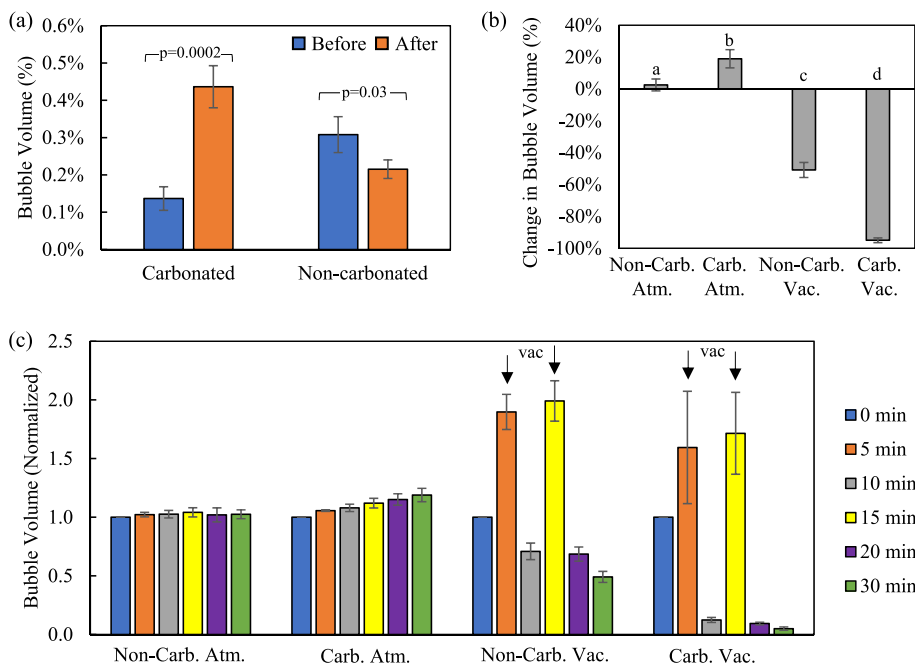


Fig. 6. Bubble volumes within VBs at different time points. (a) Effect of carbonation on the percentage of the VB volume occupied by bubbles. Bubble volume was measured before and after placing VBs in Nalgene containers for 12 h to either be carbonated or left non-carbonated ($n = 8$). (b) Effect of vacuum cycling on bubble volume. VBs were either subjected to vacuum cycling or atmospheric conditions for 30 min, with or without prior carbonation, and the resulting change in bubble volume was measured ($n = 4$). Means differ significantly ($p < 0.05$) if they do not share a common letter. (c) Bubble volumes during the course of 30 min of either vacuum cycling or atmospheric conditions, normalized to the 0-min time point ($n = 4$) with arrows indicating scans taken while under vacuum pressure.

groups showed a cycling in gas volume corresponding to the cycling of pressure. Under vacuum (5- and 15-min scans), a nearly two-fold increase in bubble volume is seen which would be expected under decreased pressures due to gas expansion. Upon return to atmospheric pressures (10- and 20-min scans), the bubble volume decreased to levels below the 0-min time point. In the case of the carbonated, vacuum-treated group, bubble volume decreased by more than 90% after 20 min. This is consistent with gas bubble expansion under vacuum causing gases to flow out of the VBs, which would lead to lower bubble volumes when the pressure returns to atmospheric. While each cycling of pressure likely removes some gas volume, the similar bubble volumes between the 10-, 20-, and 30-min time points suggests that most of the bubble volume is lost during the first vacuum cycle with less volume lost after the second and third vacuum cycles.

To test whether DMSO concentration increased over the 30-min period, the average DMSO concentration within the VB was estimated from the CT images and plotted against time. As shown in Fig. 7a, all treatment groups exhibited a significant increase in DMSO concentration over the 30 min based on regression analysis ($p < 0.02$). The atmospheric groups and non-carbonated, vacuum-treated group show increasing concentrations at each time point while the carbonated vacuum-treated group shows an overall increase but with fluctuations when under vacuum. In particular, when under vacuum at the 5- and 15-min time points, the apparent DMSO concentration was negative. Since the measured DMSO concentration is based on the grayscale intensity of the CT images (Eq. (2)), negative concentrations are a result of intensities that are lower than 0-min measurements. It is likely that the decrease in intensity observed under vacuum is caused by formation of microbubbles that are not detected during image processing. These microbubbles will lead to an overall lower VB intensity and thus a negative DMSO concentration. As the non-carbonated vacuum-treated group did not exhibit negative DMSO concentrations under vacuum, it is likely that the extra dissolved gas introduced during carbonation increased the number of microbubbles in the carbonated group, which led to the apparent negative DMSO concentrations under vacuum.

To examine whether vacuum cycling increases infiltration of DMSO into VBs, the 30-min DMSO concentrations are compared in Fig. 7b. All treatment groups yielded a similar average DMSO concentration in the VBs ranging from 2.3% to 5.6% with no significant difference between

the four treatments ($p = 0.32$). It should be mentioned that the high variation in measured DMSO concentrations, demonstrated by the wide error bars, could be masking the possible benefit of carbonation and vacuum cycling, which had an apparent DMSO concentration that was about 30% higher than the non-carbonated atmospheric group.

Even with similar DMSO concentrations across treatment groups, it is possible that different concentrations would be observed in the inner and outer regions of the VB, as the images of VBs in crystal violet dye suggest (see Fig. 5). To examine this, VBs were divided into inner and outer regions and the DMSO concentration of each was determined after 30 min. As shown in Fig. 7c, the DMSO concentration of the inner regions after 30 min was around 0% in all treatments. While the outer regions were significantly higher than the inner regions ($p = 0.0004$) with DMSO concentrations ranging from 4% to 20%, there was no difference among treatments ($p = 0.34$).

4. Discussion

There are numerous studies in food sciences that have reported significant gains in solute uptake as a result of vacuum infiltration [4,14,27,29]. We hypothesized that the benefits of vacuum infiltration could be translated to VBs and other mammalian tissues for introduction of CPAs for cryopreservation. The present study shows that vacuum infiltration led to a modest benefit of solute uptake in agarose gel while no significant differences were detected between treatments in VBs.

In food sciences, vacuum infiltration strategies often employ a single round of vacuum pressure, ranging from 2 min [37], to more than a half hour [31], followed by a hold at atmospheric pressure for anywhere from a few minutes [14], to tens of hours [4]. Even short vacuum treatment has been successful for enhancing solute penetration into foods such as fruits and vegetables. In this study, we used similar vacuum parameters, but were unable to detect improved DMSO loading into VBs. Sample microstructure, including porosity, can greatly impact the effectiveness of vacuum infiltration [5]. While the cancellous bone of VBs has a high porosity of around 80% [3,10], this pore volume is nearly completely occupied by liquid as evidenced by the gas volume fractions in the VB measured in this study, which were less than 0.5%, even after carbonation. This is a major difference from fruits and vegetables where porosity may be lower, but the pore space is nearly completely occupied

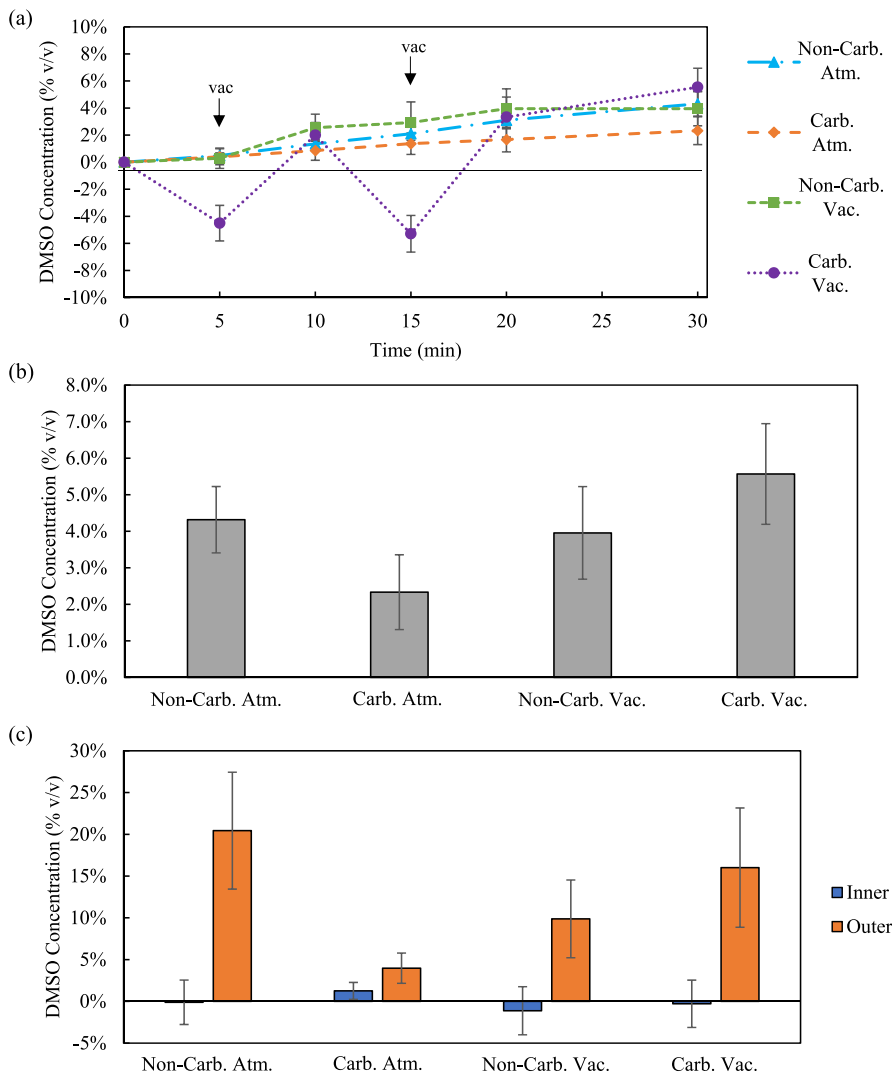


Fig. 7. DMSO concentrations in the VB measured from CT images (a) during the 30-min scan period for each treatment where arrows indicate time points where vacuum-treated groups are under vacuum pressure, (b) after 30 min of vacuum cycling or constant atmospheric conditions, and (c) in the inner (blue) and outer (orange) regions of the VB after 30 min. VBs were subjected to the following conditions ($n = 4$, all treatments): atmospheric pressure with and without prior carbonation, and vacuum cycling with and without prior carbonation. (For interpretation of the references to color in this figure legend, the reader is referred to the Web version of this article.)

by gas. For example, pears and apples have porosities of 5% and 23%, respectively [44]. Thus, vacuum infiltration may have been less effective in VBs because they contain less gas in the pore space. Studies of muscular food tissues, such as pork or fish, are consistent with this idea. Tomac et al. [41] looked at brining fish while Figueroa et al. [19] examined pork marination times using vacuum infiltration. Both saw differences in total, water, or salt mass changes between controls and vacuum treated groups but not until several hours had passed at atmospheric pressure. Such a long equilibration time would not be ideal for cryopreservation applications. Moreover, the observed differences in mass changes were modest and may not be sufficient for meaningful impacts in cryopreservation. Overall, our results suggest that vacuum infiltration may not be very effective for mammalian tissues, because they do not contain sufficient gas in their pore space. Nonetheless, it may be useful in future studies to consider a broader range of vacuum parameters and hold times, as well as other carbonation conditions, to see if this improves the results.

Based on the proposed mechanism of vacuum infiltration in foods, we hypothesized that it would be beneficial to increase the gas volume fraction by exposure to high-pressure carbon dioxide, prior to exposure to vacuum conditions. While we did see an increase in gas bubbles following carbonation, the increase was modest. We used a simple carbonation method involving dry ice that did not allow the pressure to be very precisely controlled. For future studies, it would be valuable to

develop a process allowing for more careful control of pressure, such as a closed chamber mounted with a pressure regulator. This would allow for comparison of different pressures to see if gas bubble volumes can be increased further.

Carbonation was chosen as the method to introduce gas into samples given the ubiquitous use of carbon dioxide in carbonating drinks and its success in carbonating fruits. One of the potential issues with carbon dioxide is that it can alter solution pH, which could cause cell damage. Some alternative gases that are relatively inert include nitrogen and xenon. Similar to carbon dioxide, nitrogen is readily accessible and cheap. Xenon is less readily available and more expensive. The main advantage carbon dioxide has over nitrogen and xenon is its solubility in water. Nitrogen is nearly 70x less soluble in water and xenon is almost 8x less soluble [24]. If future studies show that carbonation is damaging, it may be useful to examine more inert gases such as nitrogen or xenon.

While we did see a significant increase in dye uptake in agarose gel, the increase may not be large enough to be meaningful for CPA loading for cryopreservation. If the improvement seen for the carbonated and vacuum-treated agarose cylinders is applied to loading of 20% v/v DMSO, the resulting DMSO concentration in the tissue would only be 1% v/v higher than the atmospheric control. Such a small difference is unlikely to have a major effect on the outcome of cryopreservation. For VBs, carbonation and vacuum treatment did not have a significant effect on the measured DMSO concentrations; however, there were qualitative

differences in the pattern of dye uptake. In the cross-sectional images, the vacuum-treated VBs showed dye penetration to the inner regions, whereas dye penetration was limited to surfaces immediately exposed to the dye in atmospheric controls. Being able to introduce even a small amount of CPA throughout the sample volume would be advantageous. In contrast, the cross-sectional images of agarose following dye uptake do not show any observable penetration of dye into the inner regions. The reason for this difference in dye penetration between agarose and VBs is not yet clear and requires further study, but there are several differences between the tissues, such as mechanical properties, with agarose more closely aligning with soft tissues than bone. These results suggest that CPA loading outcomes following vacuum infiltration could be dependent on the structural and mechanical properties of tissues of interest.

This is, to our knowledge, the first work to attempt to quantify DMSO concentration within osseous tissue using CT. Previous work has validated the approach in soft tissue models including rabbit kidneys [7], bovine ovaries [6,8], and rat hearts [2]. While it was possible to estimate DMSO concentration within the bone volume, it was complicated by the presence of gas bubbles. When we examine overall trends taking into consideration bubble volumes and DMSO concentrations measured over time, the results seem to indicate that bubbles are confounding measurement of DMSO concentration, particularly for carbonated groups. Following 30 min under atmospheric conditions, carbonated VBs exhibited an increase in measured bubble volume (Fig. 6b), suggesting that bubbles are forming or growing over time. While our image processing approach aims to exclude bubbles when determining the DMSO concentration, it is unlikely that we are able to detect all of the bubbles. Undetected bubbles would be expected to erroneously lower the measured DMSO concentration. The carbonated atmospheric group had the lowest measured DMSO concentration at 30 min, approximately 2x lower than the non-carbonated atmospheric group. This is consistent with an erroneously low apparent DMSO concentration because of undetected bubbles. Furthermore, vacuum-treated, carbonated VBs exhibited apparent negative DMSO concentration when under vacuum, which is consistent with an increase in undetected bubbles when under vacuum. If bubbles are confounding DMSO concentration measurements for the carbonated groups, it is possible that the actual DMSO

concentration in the carbonated groups is higher than shown in Fig. 7.

5. Conclusions

In this work, we examined the effects of vacuum infiltration, in combination with carbonation, on CPA penetration into tissues. Agarose gel was used as a model tissue, allowing for the investigation of different vacuum conditions with and without carbonation. We saw a modest 14% increase in solute uptake when agarose gel was carbonated and subjected to vacuum cycling, compared to non-carbonated atmospheric controls. Experiments performed using human VBs employed non-invasive monitoring of bubble volume and DMSO concentration using CT imaging, allowing real-time monitoring of specimens during vacuum cycling. CT imaging of VBs showed that carbonation increased bubble volume by nearly a factor of four, while 30 min of vacuum treatment significantly decreased bubble volume for both carbonated and non-carbonated groups. This bubble volume lost during vacuum treatment was likely replaced by the surrounding DMSO solution. However, we were unable to detect significant differences in measured DMSO concentration between treatments. This could be due, at least in part, to possible confounding effects of bubbles on measurement of DMSO concentration in the carbonated groups. Overall, the present study suggests that carbonation and vacuum infiltration may cause a modest increase in solute uptake in mammalian tissues. Future studies will be necessary to determine if this increase would be sufficient for meaningful impacts in cryopreservation.

Declaration of competing interest

Wa'el Al Rawashdeh, Kimberly A. Buchanan, Erik J. Woods, and Brian H. Johnstone are employed by Ossium Health, Inc.

Acknowledgements

This work was supported by funding from the National Institutes of Health (2R44HL142418-02). We would also like to thank Jason Weist for operating the CT scanner.

Appendix

DMSO Solution Standard Curve

A linear trend between X-ray attenuation and DMSO concentration was established using a standard curve. Concentrations of DMSO from 0% to 60% (v/v) in 5% increments were made using DMSO in DI water. To make the standard curve, the average grayscale intensity of the solution volume in each well was obtained from the CT images. This was done by creating image masks of the wells in Mimics and measuring the intensity of the well ROIs in ImageJ. The X-ray attenuation proved to be proportional to the DMSO concentration (Fig. A1).

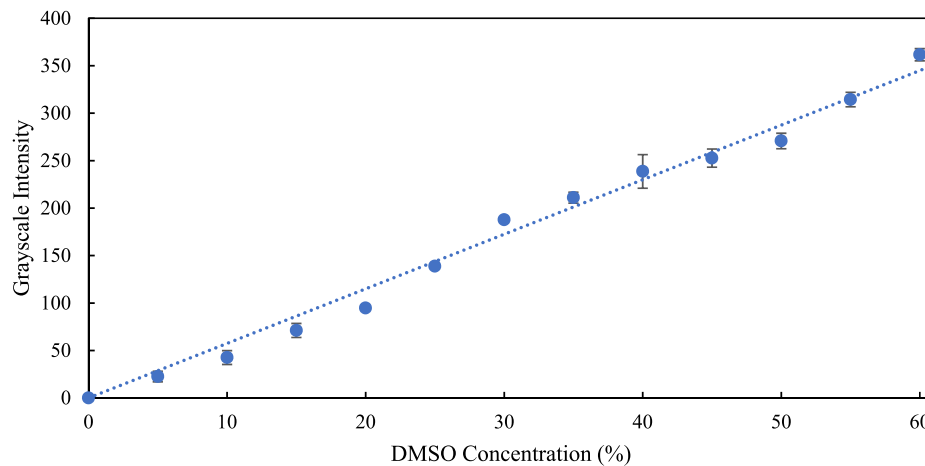


Fig. A1. The grayscale intensity of DMSO solution in well plates. The dashed line represents the best-fit line through the data points (slope = 5.75; $R^2 = 0.996$; $n = 3$).

Detecting Different DMSO Concentrations Within VBs

To confirm that DMSO at different concentrations could be detected within VBs, VBs were placed in glass beakers containing 0%, 20%, or 60% (v/v) DMSO and immediately scanned with CT. The VBs in solution were then stored at 4 °C for four weeks when they were scanned again. The 0-min and 4-week scans were analyzed, as described in Methods and Materials, to measure the VB intensity at both time points. The change in VB intensity over the 4 weeks was used in estimating the DMSO concentration within the VBs. In addition to the VB intensity, the DMSO solution within each beaker was also measured at the 0-min time point to give a solution intensity for 0%, 20%, and 60% DMSO. The slope of the intensities of the DMSO solutions represents the expected change in intensity between DMSO concentrations and was used in estimating the DMSO concentration within the VBs.

In addition to the slope and change in intensity, it is also necessary to have an idea of the porosity of the VBs as only part of the total VB volume is exchangeable with the external solution. To estimate porosity, eight VBs were dried in a drying oven at 95 °C for 18 days, at which point the changes in mass were less than 0.1% over a five-day period. Porosities were estimated using the water mass lost and the total VB volume, resulting in an estimated porosity of $55 \pm 4\%$. Eq. (A1) was used to estimate DMSO concentration within each VB:

$$\Delta \text{Intensity} = \text{Slope} * \text{Porosity} * \text{Concentration} \quad (\text{A1})$$

Fig. A2a shows the grayscale intensity for the DMSO solutions measured. The slope from the best-fit line was 4.34 grayscale intensity/DMSO concentration (%). This was lower than the slope of the best-fit line from the well-plate curve in Fig. A1. The difference in slope is thought to be a result of the container differences. The well-plate is plastic while the beakers used for the VBs in 0%, 20%, and 60% DMSO were glass, which may have resulted in beam hardening artifacts in the CT scans, altering the measured intensities of the DMSO solutions. In order to account for this, the slope from the solution intensity in glass beakers was used in Eq. (A1) instead of the slope from the well-plate standard curve.

Fig. A2b shows the results of estimating the DMSO concentration within each VB after four weeks in 0%, 20%, or 60% DMSO solution. The estimated concentration within the VBs is nearly identical to the external concentration, as expected, demonstrating that DMSO concentration can be measured within VBs based on changes in intensity.

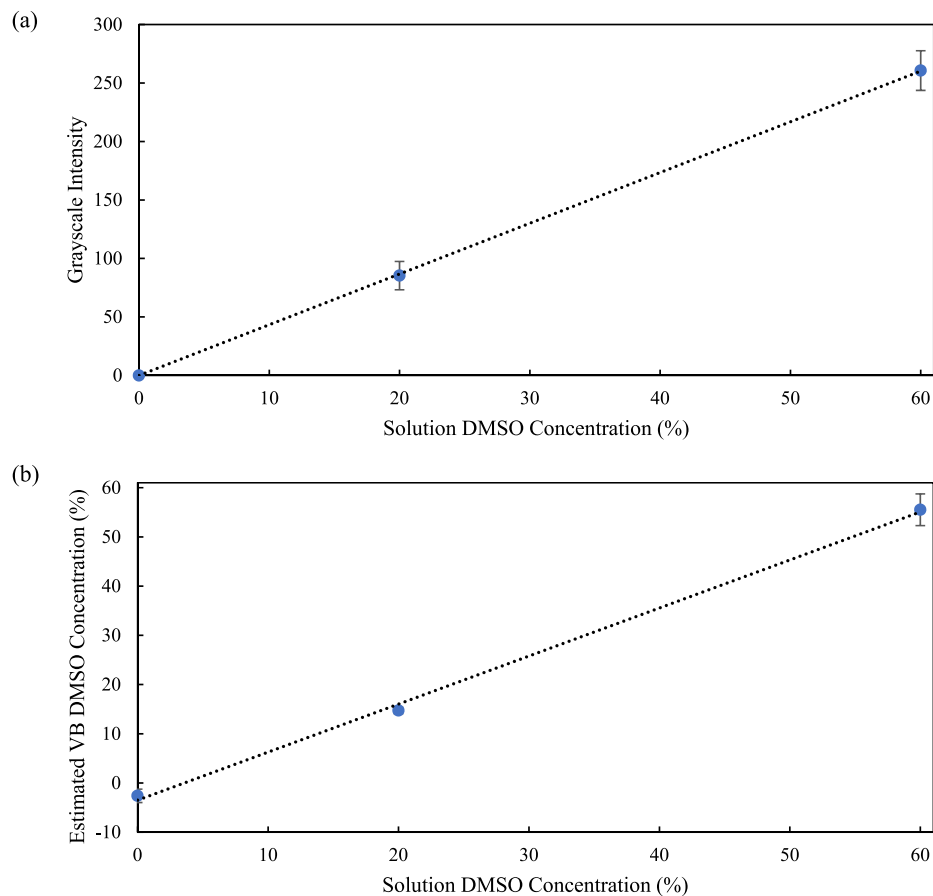


Fig. A2. a) The grayscale intensity for the DMSO solutions in the glass beakers at the 0-min time point. The dashed line represents the best-fit line (slope = 4.34; $R^2 = 1$). b) The estimated DMSO concentration within the VBs after 4 weeks, plotted against the external solution DMSO concentration. The dashed line represents the best-fit line (slope = 0.98; $R^2 = 0.999$). Data points represent mean \pm SEM; $n = 3$.

Consistency Between Scans

PBS and DMSO solutions were included in the VB scans to provide a consistent image control between scans. Each scan had two containers of PBS and two containers of 40% DMSO solution to allow for comparisons of the same solution across scans. For each container, the average intensity of the solution was measured. Fig. A3 shows the results of the intensity measurements of both PBS and DMSO containers. The results show that each container measured similarly within a 30-min window but there is potential for variability in scan measurements between weeks. For example, one of the PBS containers had an intensity that differed by approximately five grayscale units between weeks, which would correspond to a DMSO concentration of approximately 1%. Lastly, the difference in intensity between the PBS and 40% DMSO solutions is approximately what would be expected based on Fig. A1.

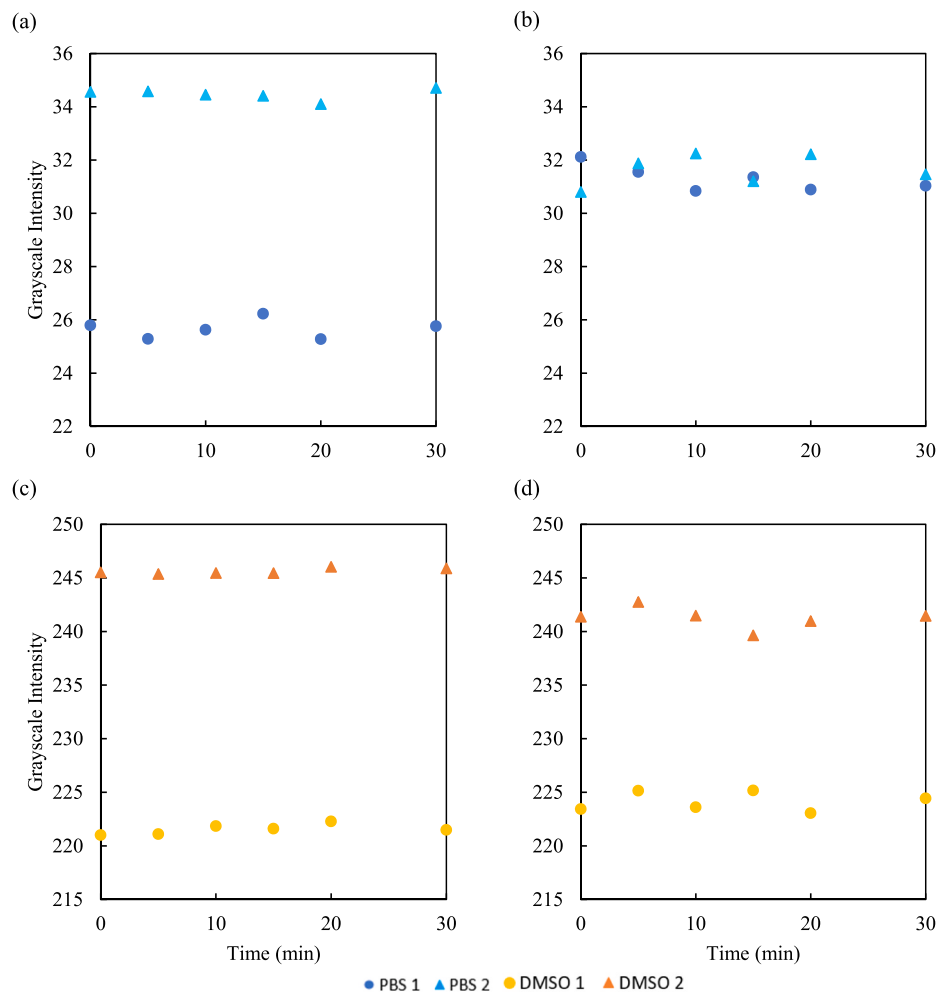


Fig. A3. (a,b) Grayscale intensity for PBS containers 1 and 2 in scans taken one week apart during the 30-min experimental time. (c,d) Grayscale intensity for DMSO containers 1 and 2 in scans taken one week apart during the 30-min experimental time.

References

- [1] G. Bedoschi, K. Oktay, Current approach to fertility preservation by embryo cryopreservation, *Fertil. Steril.* 99 (2013) 1496–1502.
- [2] N. Bleisinger, R. Dittrich, O. Strahl, R. Brauweiler, I. Hoffmann, M.W. Beckmann, T. Volk, Me2SO perfusion time for whole-organ cryopreservation can be shortened: results of micro-computed tomography monitoring during Me2SO perfusion of rat hearts, *PLoS One* 15 (2020), e0238519.
- [3] A. Boccaccio, P. Vena, D. Gastaldi, G. Franzoso, R. Pietrabissa, C. Pappalettere, Finite element analysis of cancellous bone failure in the vertebral body of healthy and osteoporotic subjects, *Proc. Inst. Mech. Eng. H* 222 (2008) 1023–1036.
- [4] S. Chen, M. Zhang, S. Wang, Physiological and quality responses of Chinese ‘Suli’ pear (*Pyrus bretschneideri* Rehd.) to 1-MCP vacuum infiltration treatment, *J. Sci. Food Agric.* 90 (2010) 1317–1322.
- [5] A. Chiralt, P. Fito, J.M. Barat, A. Andrés, C. González-Martínez, I. Escriche, M. M. Camacho, Use of vacuum impregnation in food salting process, *J. Food Eng.* 49 (2001) 141–151.
- [6] A. Corral, M. Balcerzyk, M. Gallardo, C.A. Amorim, Á. Parrado-Gallego, R. Risco, An optimized controlled rate slow cooling protocol for bovine ovarian tissue cryopreservation by means of X-ray computed tomography, *Theriogenology* 119 (2018) 183–188.
- [7] A. Corral, M. Balcerzyk, Á. Parrado-Gallego, I. Fernández-Gómez, D.R. Lamprea, A. Olmo, R. Risco, Assessment of the cryoprotectant concentration inside a bulky organ for cryopreservation using X-ray computed tomography, *Cryobiology* 71 (2015) 419–431.
- [8] A. Corral, M. Clavero, M. Gallardo, M. Balcerzyk, C.A. Amorim, Á. Parrado-Gallego, M.-M. Dolmans, F. Paulini, J. Morris, R. Risco, Ovarian tissue cryopreservation by stepped vitrification and monitored by X-ray computed tomography, *Cryobiology* 81 (2018) 17–26.
- [9] S. Crippa, L. Santi, M. Berti, G. De Ponti, M.E. Bernardo, Role of ex vivo expanded mesenchymal stromal cells in determining hematopoietic stem cell transplantation outcome, *Front. Cell Dev. Biol.* 9 (2021) 821.
- [10] C. Daish, R. Blanchard, K. Gulati, D. Losic, D. Findlay, D.J.E. Harvie, P. Pivonka, Estimation of anisotropic permeability in trabecular bone based on microCT imaging and pore-scale fluid dynamics simulations, *BoneKey Rep.* 6 (2017) 129–139.
- [11] Y. Deng, Y. Zhao, Effects of pulsed-vacuum and ultrasound on the osmodehydration kinetics and microstructure of apples (Fuji), *J. Food Eng.* 85 (2008) 84–93.
- [12] Department of Health and Human Services, Health Resources and Services Administration, Annual Report of the U.S. Organ Procurement and Transplantation Network and the Scientific Registry of Transplant Recipients: Transplant Data 2008–2019, Healthcare Systems Bureau, Division of Transplantation, Rockville, MD, 2019. United Network for Organ Sharing, Richmond, VA; University Renal Research and Education Association, Ann Arbor, MI, 2019.
- [13] Y. Ding, J. Shao, J. Li, Y. Zhang, K. Hong, K. Hua, X. Wang, Successful fertility following optimized perfusion and cryopreservation of whole ovary and allotransplantation in a premature ovarian insufficiency rat model, *J. Ovarian Res.* 11 (2018) 35.
- [14] Y. Duarte-Correa, A. Díaz-Osorio, J. Osorio-Arias, P.J.A. Sobral, O. Vega-Castro, Development of fortified low-fat potato chips through vacuum impregnation and microwave vacuum drying, *Innovat. Food Sci. Emerg. Technol.* 64 (2020), 102437.
- [15] European Commission, Commission Regulation (EU) No 231/2012 of 9 March 2012 Laying Down Specifications for Food Additives Listed in Annexes II and III to Regulation (EC) No 1333/2008 of the European Parliament and of the Council Text with EEA Relevance, (n.d.).
- [16] M.D. Fahmy, K.A. Almansoori, L. Laouar, V. Prasad, L.E. McGann, J.A.W. Elliott, N. M. Jomha, Dose–injury relationships for cryoprotective agent injury to human chondrocytes, *Cryobiology* 68 (2014) 50–56.
- [17] G.M. Fahy, B. Wovk, R. Pagotan, A. Chang, J. Phan, B. Thomson, L. Phan, Physical and biological aspects of renal vitrification, *Organogenesis* 5 (2009) 167–175.
- [18] G.M. Fahy, B. Wovk, J. Wu, J. Phan, C. Rasch, A. Chang, E. Zendejas, Cryopreservation of organs by vitrification: perspectives and recent advances, *Cryobiology* 48 (2004) 157–178.

- [19] C. Figueroa, C. Ramírez, H. Núñez, A. Jaques, R. Simpson, Application of vacuum impregnation and CO₂-laser microperforations in the potential acceleration of the pork marinating process, *Innovat. Food Sci. Emerg. Technol.* 66 (2020), 102500.
- [20] P. Fito, A. Andrés, A. Chiralt, P. Pardo, Coupling of hydrodynamic mechanism and deformation-relaxation phenomena during vacuum treatments in solid porous food-liquid systems, *J. Food Eng.* 27 (1996) 229–240.
- [21] P. Fito, A. Chiralt, J.M. Barat, A. Andrés, J. Martínez-Monzó, N. Martínez-Navarrete, Vacuum impregnation for development of new dehydrated products, *J. Food Eng.* 49 (2001) 297–302.
- [22] Z. Gao, B. Namsrai, Z. Han, P. Joshi, J.S. Rao, V. Ravikumar, A. Sharma, H.L. Ring, D. Idiyatullin, E.C. Magnuson, P.A. Iaizzo, E.G. Tolkacheva, M. Garwood, Y. Rabin, M. Etheridge, E.B. Finger, J.C. Bischof, Vitrification and Rewarming of Magnetic Nanoparticle-Loaded Rat Hearts, *Advanced Materials Technologies*, 2021 n/a.
- [23] V.S. Gorantla, S. Schneeberger, L.R. Moore, V.S. Donnenberg, L. Zimmerlin, W.P. A. Lee, A.D. Donnenberg, Development and validation of a procedure to isolate viable bone marrow cells from the vertebrae of cadaveric organ donors for composite organ grafting, *Cytotherapy* 14 (2012) 104–113.
- [24] W.M. Haynes, *CRC Handbook of Chemistry and Physics*, CRC Press LLC, Baton Rouge, UNITED STATES, 2011.
- [25] B.H. Johnstone, F. Messner, G. Brandacher, E.J. Woods, A large-scale bank of organ donor bone marrow and matched mesenchymal stem cells for promoting immunomodulation and transplant tolerance, *Front. Immunol.* 12 (2021), 622604.
- [26] B.H. Johnstone, H.M. Miller, M.R. Beck, D. Gu, S. Thirumala, M. LaFontaine, G. Brandacher, E.J. Woods, Identification and characterization of a large source of primary mesenchymal stem cells tightly adhered to bone surfaces of human vertebral body marrow cavities, *Cytotherapy* 22 (2020) 617–628.
- [27] A. Joshi, A. Kar, S.G. Rudra, V.R. Sagar, E. Varghese, M. Lad, I. Khan, B. Singh, Vacuum impregnation: a promising way for mineral fortification in potato porous matrix (potato chips), *J. Food Sci. Technol.* 53 (2016) 4348–4353.
- [28] E.C.R. Leonel, A. Corral, R. Risco, A. Camboni, S.R. Taboga, P. Kilbride, M. Vazquez, J. Morris, M.-M. Dolmans, C.A. Amorim, Stepped vitrification technique for human ovarian tissue cryopreservation, *Sci. Rep.* 9 (2019), 20008.
- [29] X. Lin, C. Luo, Y. Chen, Effects of vacuum impregnation with sucrose solution on mango tissue, *J. Food Sci.* 81 (2016) E1412–E1418.
- [30] J.E. Lozano, C. Anon, G.V. Barbosa-Canovas, E. Parada-Arias, *Trends in Food Engineering*, CRC Press, 2000.
- [31] J. Mao, L. Zhang, F. Chen, S. Lai, B. Yang, H. Yang, Effect of vacuum impregnation combined with calcium lactate on the firmness and polysaccharide morphology of kyoho grapes (*Vitis vinifera* x *V. Labrusca*), *Food Bioprocess Technol.* 10 (2017) 699–709.
- [32] P. Mazur, *Cryobiology: the freezing of biological systems*, *Science* 168 (1970) 939–949.
- [33] H. Mújica-Paz, A. Valdez-Fragoso, A. López-Malo, E. Palou, J. Welti-Chanes, Impregnation and osmotic dehydration of some fruits: effect of the vacuum pressure and syrup concentration, *J. Food Eng.* 57 (2003) 305–314.
- [34] K. Oktay, A.P. Cil, H. Bang, Efficiency of oocyte cryopreservation: a meta-analysis, *Fertil. Steril.* 86 (2006) 70–80.
- [35] A. Prystalov, O. Bobrova, L. Kuleshova, Application of vacuum infiltration in cryopreservation of isolated grape buds, *Problems of Cryobiology and Cryomedicine* 31 (2021) 51–57.
- [36] P.H. Purdy, A review on goat sperm cryopreservation, *Small Rumin. Res.* 63 (2006) 215–225.
- [37] A. Quintanilla, A. Mencía, J. Powers, B. Rasco, J. Tang, S.S. Sablani, Vacuum impregnation of firming agents in red raspberries, *J. Sci. Food Agric.* 98 (2018) 3706–3714.
- [38] X.Q. Shi, P. Fito, A. Chiralt, Influence of vacuum treatment on mass transfer during osmotic dehydration of fruits, *Food Res. Int.* 28 (1995) 445–454.
- [39] K. Soejima, K. Shimoda, M. Takeuchi, T. Yamaki, T. Kono, H. Sakurai, H. Nakazawa, Preliminary report of novel technique for cryopreservation—vacuum-assisted cryoprotectant infiltration, *Cryobiology* 65 (2012) 21–26.
- [40] A. Tejo-Otero, F. Fenollosa-Artés, I. Achaerandio, S. Rey-Vinolas, I. Buj-Corral, M.Á. Mateos-Timoneda, E. Engel, Soft-tissue-mimicking using hydrogels for the development of phantoms, *Gels* 8 (2022) 40.
- [41] A. Tomac, S. Rodríguez Mallo, S. Perez, A.B. Garcia Loreda, M.I. Yeannes, Vacuum impregnation in *Merluccius hubbsi* hake fillets brining. Effect on mass transfer kinetics, texture and colour, *Lebensm. Wiss. Technol.* 119 (2020), 108892.
- [42] C. Toyama-Mori, K. Suzuki, Y. Miyazaki, T. Suzuki, M. Katsumata, K. Tanaka, M. Usami, T. Takizawa, Negative air pressure treatment accelerates the penetration of permeable cryoprotectants into bovine ovarian tissue in vitrification protocol and improves cell density after vitrification, *Cryobiology* 88 (2019) 92–97.
- [43] C.T. Vangsness Jr., G. Higgs, J.K. Hoffman, J. Farr, P.A. Davidson, F. Milstein, S. Geraghty, Implantation of a novel cryopreserved viable osteochondral allograft for articular cartilage repair in the knee, *J. Knee Surg.* 31 (2018) 528–535.
- [44] P. Verboven, G. Kerckhofs, H.K. Mebatsion, Q.T. Ho, K. Temst, M. Wevers, P. Cloetens, B.M. Nicolai, Three-dimensional gas exchange pathways in pome fruit characterized by synchrotron X-ray computed tomography, *Plant Physiol.* 147 (2008) 518–527.
- [45] R.M. Warner, E. Ampo, D. Nelson, J.D. Benson, A. Eroglu, A.Z. Higgins, Rapid quantification of multi-cryoprotectant toxicity using an automated liquid handling method, *Cryobiology* 98 (2021) 219–232.
- [46] E.J. Woods, A.M. Sherry, J.R. Woods, J.W. Hardin, M. LaFontaine, G. Brandacher, B.H. Johnstone, Ischemia considerations for the development of an organ and tissue donor derived bone marrow bank, *J. Transl. Med.* 18 (2020) 300.
- [47] M. Yeste, Sperm cryopreservation update: cryodamage, markers, and factors affecting the sperm freezability in pigs, *Theriogenology* 85 (2016) 47–64.
- [48] E.S. Yolcu, H. Shirwan, N. Askenasy, Mechanisms of tolerance induction by hematopoietic chimerism: the immune perspective, *STEM CELLS Translational Medicine* 6 (2017) 700–712.